Bull. Mater. Sci., Vol. 34, No. 4, July 2011, pp. 915–920. © Indian Academy of Sciences.

Dielectric relaxation and ionic conductivity studies of $Na_2ZnP_2O_7$

S CHOUAIB*, A BEN RHAIEM and K GUIDARA
Laboratoire de L'Etat Solide, Faculté des Sciences, de Sfax-BP 1171-3000 Sfax, Tunisia

MS received 10 December 2009; revised 28 January 2010

Abstract. **The $Na_2ZnP_2O_7$ compound was obtained by the conventional solid-state reaction. The sample was characterized by X-ray powder diffraction, infrared analysis and electrical impedance spectroscopy. The impedance plots show semicircle arcs at different temperatures and an electrical equivalent circuit has been proposed to explain the impedance results. The circuits consist of the parallel combination of bulk resistance R_p and constant phase elements CPE. Dielectric data were analyzed using complex electrical modulus M^* for the sample at various temperatures. The frequency dependence of the conductivity is interpreted in terms of Jonscher's law. The conductivity $\sigma_{d.c.}$ follows the Arrhenius relation. The near value of activation energies obtained from the analysis of M'' and conductivity data confirms that the transport is through ion hopping mechanism, dominated by the motion of the Na^+ ions in the structure of the investigated materials.**

Keywords. **Equivalent circuit; electrical modulus; a.c. conductivity; hopping mechanism.**

1. Introduction

Double phosphates of $A_2BP_2O_7$ formulation containing simultaneously an alkaline ion (A^+) and a divalent cation (B^{2+}) form a large family of materials (El Maadi *et al* 1995; Erragh *et al* 1995; Erragh *et al* 1998; Sanz *et al* 1999; Belharouak *et al* 2000; Dridi *et al* 2000; Dridi *et al* 2001). The structure of these phosphates which have been the object of a single crystal structure investigation are diverse, and it is difficult to classify these materials as a function of classical fundamental criteria such us cation size, coordination number or chemical bonding. Selecting the Na^+ and Zn^{2+} cations as A^+ and B^{2+} ions, respectively, are interested, in the present work.

The crystal structure of $Na_2ZnP_2O_7$ has been determined by X-ray diffraction using single crystals. This compound crystallized in the tetragonal system with the space group $P4_2/n$ and unit cell parameters: $a = b =$ 21·771 Å and $c =$ 10·285 Å. The structure is made up of $[ZnP_2O_7]$ layers consisting of corners sharing $[P_2O_7]$ groups and $[ZnO_4]$ tetrahedral, and the sodium atoms are located between the layers in 7- or 8-fold coordinated sites (figure 1) (Belharouak *et al* 2000).

In the present work, we propose to investigate the electrical and dielectrical properties of the $Na_2ZnP_2O_7$ compound as a function of frequency and temperature.

2. Experimental

The $Na_2ZnP_2O_7$ compound was synthesized by the classic ceramic method. Stoichiometric quantities of Na_2CO_3, ZnO and $(NH_4)_2HPO_4$ were well ground, mixed, and progressively heated first to 523 K to expel NH_3 and H_2O and then to 623 K.

X-ray powder diffraction pattern was recorded using a Philips PW 1710 diffractometer operating with copper radiation $K_\alpha =$ 1·5418 Å. Units cells parameters of the synthesized compound have been refined by the least square method from the powder data.

The infrared absorption spectrum of crystalline powders in KBr was recorded on a FT–IR 470 Shymadzu spectrophotometer in 400–1300 cm^{-1} range.

The electrical measurements were performed using a two-electrode configuration. The polycrystalline $Na_2ZnP_2O_7$ sample was pressed into pellets of 8 mm diameter and 0·8 mm thickness using 3t/cm^2 uniaxial pressure. Electrical impedances were measured in the frequency ranging from 200 Hz to 5 MHz with the TEGAM 3550 ALF automatic bridge monitored by a microcomputer between 600 and 690 K.

3. X-ray powder analysis

The X-ray powder diffractogram (figure 2) reveals that the synthesized compound crystallizes in the tetragonal system with the space group $P4_2/n$ and the refined unit cell parameters are: $a = b =$ 21·775 Å and $c =$ 10·287 Å, which are in good agreement with the literature values (Dridi *et al* 2001).

4. Infrared absorption spectroscopy

The infrared spectrum of the $Na_2ZnP_2O_7$ compound at room temperature is shown in figure 3. A detailed

*Author for correspondence

assignment of all bands is difficult but we can attribute some of them by comparison with similar compounds (Santha *et al* 1993; Mahadevan Pillai *et al* 1999; Kuhlmann *et al* 2001). The principal bands are assigned to the internal modes of (P_2O_7) group: two bands are observed at 1176 and 1086 cm^{-1}, which were assigned respectively to the ν_{as} (PO_3) and ν_s (PO_3) modes. The two strong bonds observed at 916 and 722 cm^{-1} were assigned to asymmetric ν_{as} (POP) and symmetric ν_s (POP) stretching vibrations of bridging (P–O–P) modes. A smaller one, assigned to the symmetrical (POP) deformation mode δ_s (POP) arises near 530 cm^{-1}. Two bands are observed at 626 and 550 cm^{-1} were assigned respectively to the δ_{as} (PO_3) and δ_s (PO_3) deformation modes. Another band, assigned to the (PO_3) rocking ρ_r (PO_3), was observed near 498 cm^{-1}.

Note that one of the most interesting aspects of this study is the ability to obtain direct information about the configuration of the P–O–P bridges. The symmetric POP stretching mode δ_s (POP) confirms the presence of the diphosphate group in the compound.

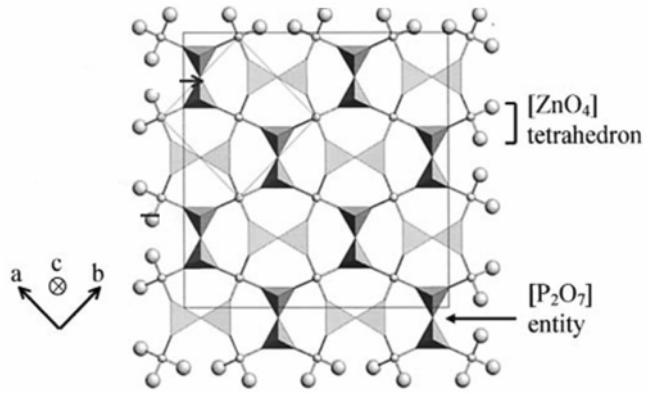

Figure 1. Projection of the $Na_2ZnP_2O_7$ structure on the (a, b) plan.

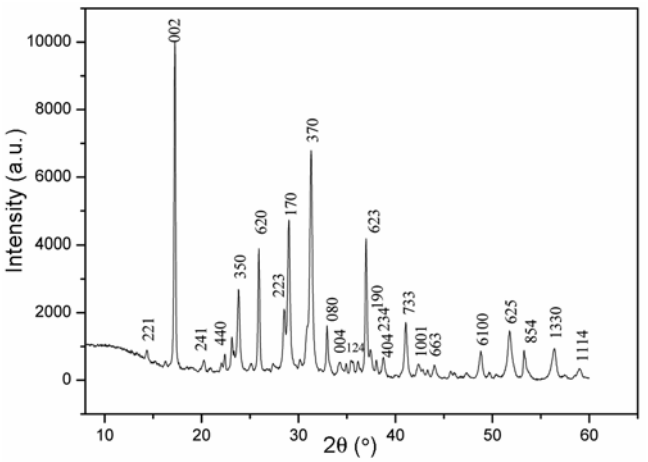

Figure 2. X-ray diffractogram of $Na_2ZnP_2O_7$ compound.

5. Dielectric study

5.1 *Impedance spectrum analysis*

Figure 4 shows the complex impedance spectra of $Na_2ZnP_2O_7$ for some representative temperatures. The

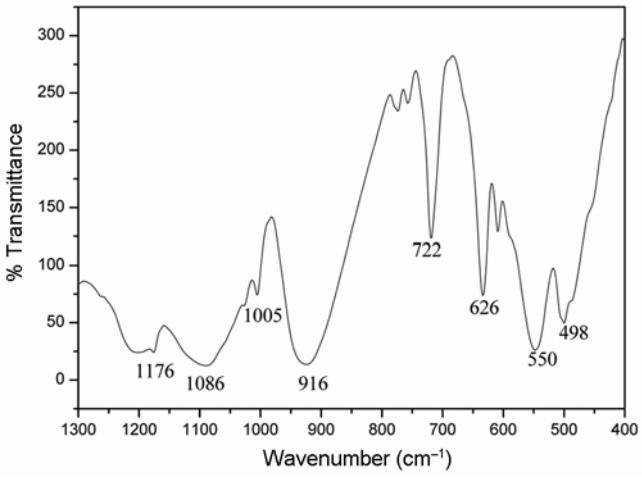

Figure 3. Infrared spectra of the $Na_2ZnP_2O_7$ compound.

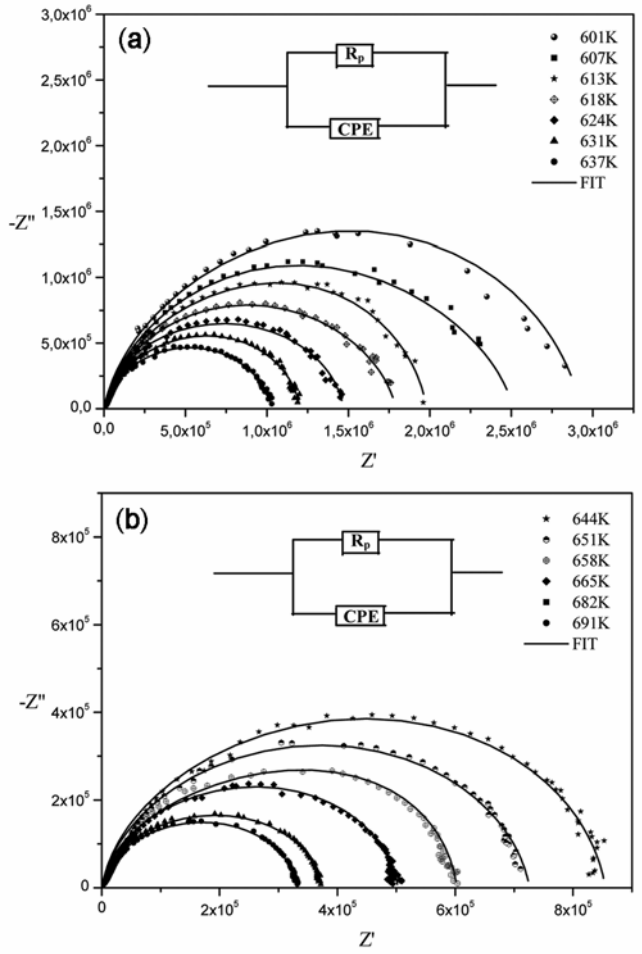

Figure 4. Experimental and simulated semicircles plots at different temperatures.

spectra are characterized by the appearance of semi-circle arcs whose pattern changes, but not its shape, when the temperature is increased. Such pattern tells us about the electrical process occurring within the sample and their correlation with the sample microstructure when modeled in terms of an electrical equivalent circuit (Ben Rhaiem *et al* 2005; Nadeem *et al* 2005; Parathan *et al* 2005). The equivalent circuit configuration for the impedance plan plot is the resistance R_p (bulk resistance) and in the terms of complex elements: constant phase elements (capacity of the fractal interface CPE). The impedance of CPE is

$$Z_{CPE} = 1/Q(j\omega)^{\alpha}, \quad (1)$$

where Q indicates the value of capacitance of the CPE element and α is the fractal exponent. Further, (1) shows that as $\alpha \to 1$, $Z_{CPE} \to 1/jQ\omega$, involving a pure capacitance, and as $\alpha \to 0$, $Z_{CPE} \to 1/Q$, a pure conductance.

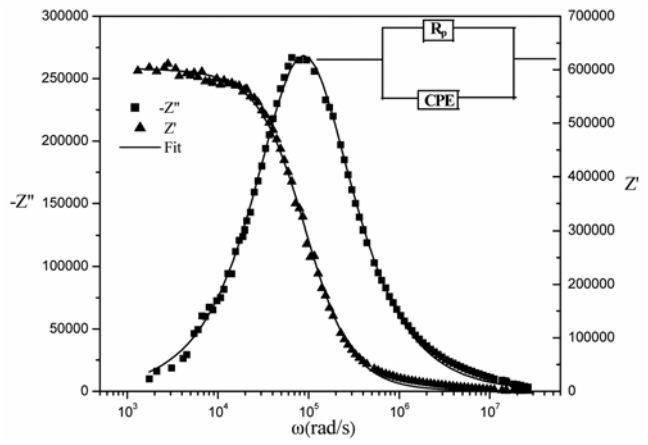

Figure 5. Variation of Z' and $-Z''$ with angular frequency at 685 K.

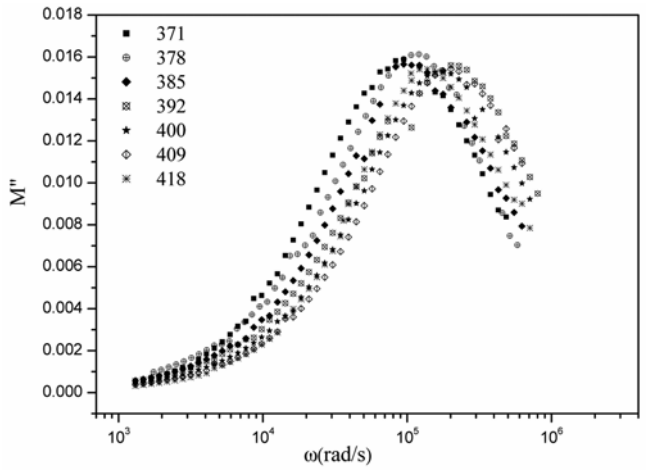

Figure 6. Angular frequency dependence of the imaginary part of electric modulus at several temperatures.

The real and imaginary components of the whole impedance of this circuit were calculated according to the following expressions:

$$Z' = \frac{R_p^2 Q\omega^{\alpha}\cos(\alpha\pi/2) + R_p}{(1 + R_p Q\omega^{\alpha}\cos(\alpha\pi/2))^2 + (R_p Q\omega^{\alpha}\sin(\alpha\pi/2))^2}, \quad (2)$$

$$-Z'' = \frac{R_p^2 Q\omega^{\alpha}\sin(\alpha\pi/2)}{(1 + R_p Q\omega^{\alpha}\cos(\alpha\pi/2))^2 + (R_p Q\omega^{\alpha}\sin(\alpha\pi/2))^2}, \quad (3)$$

Z', $-Z''$ data measured at 685 K and their fits according to the above equations versus frequency are represented in figure 5. The good conformity of calculated lines with the experimental measurement indicates that the suggested

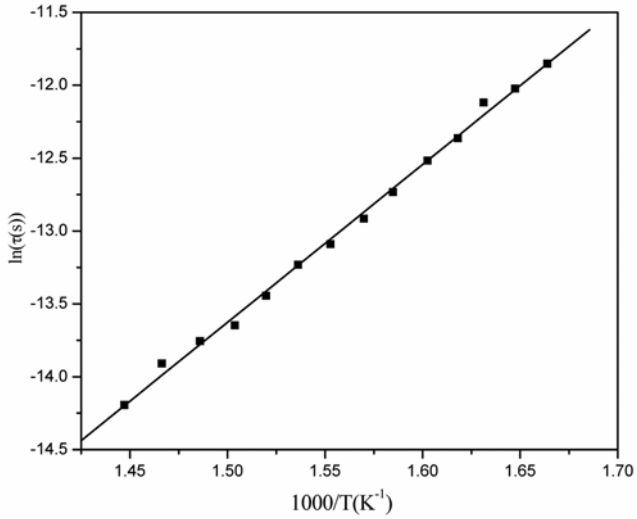

Figure 7. Temperature dependence of relaxation time $\tau(s)$.

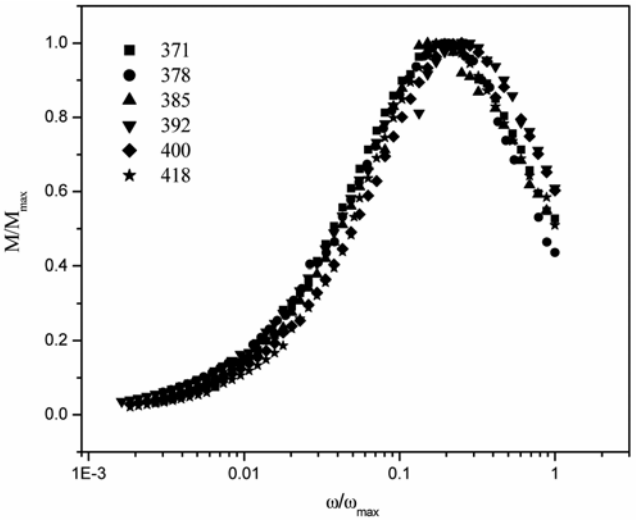

Figure 8. M''/M''_{max} versus (ω/ω_{max}) at various temperatures.

Table 1. Temperature dependence of α, Q and R_p.

T (K)	601	613	618	631	651	665	673	682	691
α	0·90	0·93	0·91	0·92	0·92	0·93	0·92	0·93	0·93
Q (pF)	45·14	35·62	44·33	37·85	42·74	39·46	39·34	39·34	40·01
R_p (Ω)	2923843	1979207	1791261	1204432	726134	502556	431817	372073	331796

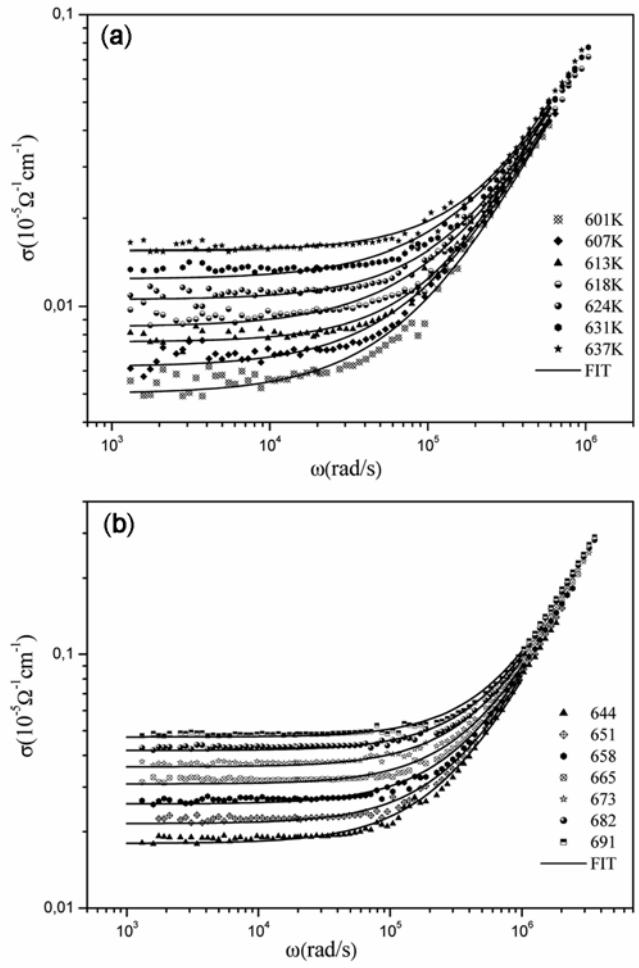

Figure 9. Angular frequency dependence of the a.c. conductivity at various temperatures.

equivalent circuit describes the crystal–electrolyte interface reasonably well.

Fitted values of R_p, Q and α parameters for different temperature are listed in table 1. It is obvious that all the capacitance values (Q) are in the range of pF. This implies that the single semicircular response is from grain interiors, which is expected from the sample where no grain boundaries are involved. The values of α vary in the range 0·9–1 confirming the weakness interaction between localized sites.

5.2 *Modulus studies*

The modulus formalism is particularly suitable to extract phenomena such as electrode polarisation (Hodgeet *et al* 1976; Ganguli *et al* 1999; Lenfredi *et al* 2002) and conductivity relaxation times (Chen *et al* 1993; Reau *et al* 1997; Ghosh *et al* 2002; Lenfredi *et al* 2002). The complex electric modulus can be represented by the following equation

$$M^* = \frac{1}{\varepsilon^*} = j\omega C_0 Z^*, \tag{4}$$

where C_0 is the vacuum capacitance of the cell.

Figure 6 shows the variation of imaginary part of electric modulus as a function angular frequency at different temperatures. In the M'' plot, the peaks are broader and asymmetric on both sides of the maxima then predicted by ideal Debye behaviour. The frequency range where the peak occurs is indicative of the transition from long range to short range mobility. As temperature increases, the modulus peak maxima (ω_m) move toward higher frequency, where ω_m is the most probable relaxation rate, and is related to the most probable ion relaxation time, τ, by the relation of $\omega_m \tau = 1$. The obtained temperature dependence of the relaxation time is plotted in figure 7. It shows that the relaxation time appears thermally activated and can be described by Arrhenius law $\tau = \tau_0 \exp(E_m/k_B T)$, where τ_0 is the pre-exponential factor ($\tau_0 = 2{\cdot}43 \times 10^{-4}$s), E_m is the activation energy from modulus (E_m = 0·96 eV) and k_B is Boltzmann's constant.

Figure 8 shows the normalized plot of M''/M''_{max} versus (ω/ω_{max}) at various temperatures. The normalised plot shows that all the curves for different temperature overlap a single master curve. This suggests that all possible relaxation mechanisms occurring at different frequencies exhibit the same thermal energy and the dynamical processes are temperature-independent. The modulus plot can be characterized by full width at half height or in terms of a nonexponential decay function (Sural and Gosh 2000; Gómez *et al* 2001; Anantha and Hariharan 2005; Padmasree *et al* 2006)

$$\varphi(t) = \exp(-t/\tau)^{\beta} \ (0 < \beta < 1), \tag{5}$$

where τ is the characteristic relaxation time and β is the well known Kohlrausch parameter, which decreases with an increase in the relaxation time distribution. The β value can be determinated by knowing the full width at half height (FWHH) of the M''/M''_{max} plot (β = 1·14/FWHH = 0·79).

5.3 *Electrical conductivity analysis*

The angular frequency dependence of a.c. conductivity at various temperatures for the sample is shown in figure 9.

Table 2. E_C, β and $\sigma_{d.c.}$ parameters.

	$Na_2ZnP_2O_7$	$AgNaZnP_2O_7$ [28]	$Ag_2ZnP_2O_7$ [29]
E_C (eV)	0·94	0·79	0·72
β	0·79	0·74	0·65
$\sigma_{d.c.}$ (Ω^{-1} cm^{-1})	$\sigma_{600\ K} = 4{\cdot}98 \times 10^{-8}$	$\sigma_{550\ K} = 1{\cdot}39 \times 10^{-7}$	$\sigma_{550\ K} = 3{\cdot}31 \times 10^{-5}$

The data shows a frequency-independent conductivity for low frequencies and followed by an increase in conductivity for high frequency, quite similar to the vast majority of solids. The phenomena of the conductivity dispersion in solids are generally analyzed using Jonscher's power law:

$$\sigma_{ac}(\omega) = \sigma_{d.c.} + A\omega^n,$$

where $\sigma_{d.c.}$ is the direct current conductivity of the sample, A is a constant for a particular temperature and n is the power exponent.

The exponent n represents the degree of interaction between mobile ions and the environments surrounding them. The transport mechanism is explained by the thermally activated hopping process between two sites separated by an energy barrier. The above equation has been used to fit the a.c. conductivity data. In the fitting procedure, A and n values have been varied simultaneously to get the best fits.

A plot of $-\ln(A)$ against n (figure 10) indicates a linear temperature-independent and structure-insensitive correlation between the values of these two parameters. Such behaviour was observed in different types of materials and varied transport mechanism (Jonscher 1977; Louati *et al* 2005; Papathanassiou 2005).

D.C. conductivity data are plotted in Arrhenius format as $\ln(T\sigma_{dc})$ vs $1000/T$ (figure 11) and show Arrhenius-type behaviour described by

$$T\sigma_{d.c.} = B\exp(-E_c/kT), \quad (7)$$

where B ($B = 1{\cdot}126\ 10^6\ \Omega^{-1}$ cm^{-1} K) is the pre-exponential factor. The activation energy for conduction ($E_C = 0.94$ eV) is almost the same as that of the activation energy for the relaxation process ($E_m = 0{\cdot}93$ eV). The near value of activation energies obtained from the analyses of M'' and conductivity data confirms that the transport is through ion hopping mechanism in the investigated material.

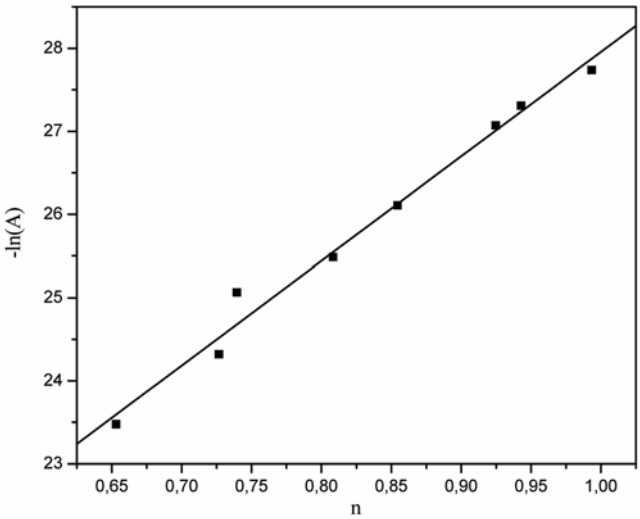

Figure 10. Plot of $-\ln(A)$ vs n.

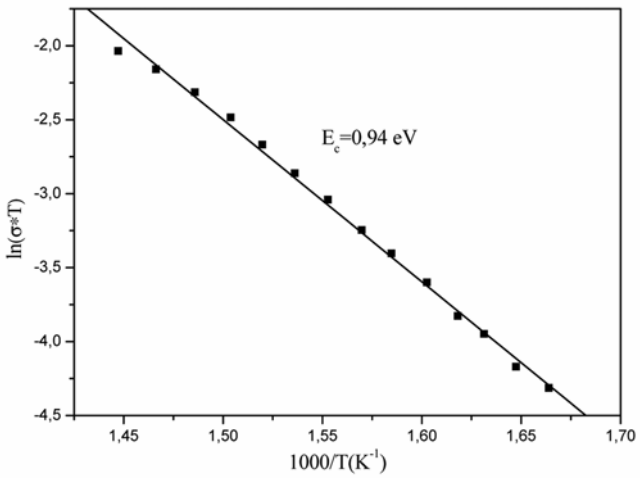

Figure 11. Plot of d.c. conductivity $\sigma_{d.c.}$ vs $1000/T$.

6. Discussion

In an earlier report we have studied the a.c. conductivity and dielectric behaviour of $Zn_2P_2O_7$ compound as a function of temperature and frequency. The correlation between the CBH model and the crystallographic results permit us to deduce that the conduction is probably due to the motion of Zn^{2+} in the cationic layers and/or a long c-direction. This compound showed a very low ionic conductivity, when the $\sigma_{d.c.} = 2 \times 10^{-7}\ \Omega^{-1}$ cm^{-1} at 730 K (Jarboui *et al* 2010).

Furthermore, we successfully introduced a monovalent cation into the $Zn_2P_2O_7$ compound and we have synthesized the $A_2ZnP_2O_7$ (A = Ag and/or Na) compounds. The ionic conductivity of $Ag_2ZnP_2O_7$, $AgNaZnP2O_7$ and $Na_2ZnP_2O_7$ compounds are characterized by the hopping of the Na^+ and/or Ag^+ ions (Ben Rhaiem *et al* 2009a, b).

The low frequency limit $\sigma_{d.c.}$ of the bulk $\sigma_{a.c.}$ conductivity determined by impedance spectroscopy is governed mainly by the hoping rate of free charge carriers and the charge carrier concentration $N(T)$

$$\sigma_{d.c.} = e^2 N(T)\ \gamma a_h^2\ (\nu_0/kT)\ \exp(S_\mu/k)\exp(-E_\mu/kT), \quad (11)$$

where a_h is the hopping distance; γ is a geometrical factor equal to 1/6 for isotropic media; ν_0 is an attempt frequency to overcome the potential barrier; S_μ is the migration entropy; E_μ is the migration energy; the other parameters having their conventional meaning (Almond *et al* 1987; Uvarovet *et al* 1994).

Identifying E_μ to E_c the pre-exponential factor B is

$$B = (e^2 a_h^2 \nu_0/6k)N(T)\exp(S_\mu/k). \quad (12)$$

The electrical properties of $Na_2ZnP_2O_7$, $AgNaZnP_2O_7$ and $Ag_2ZnP_2O_7$ are compared in table 2. The better properties obtained for $Ag_2ZnP_2O_7$ can be attributed to

- The number of charge carriers $N(T)$ participating in conductivity phenomena in $Ag_2ZnP_2O_7$ is very superior than that observed in the studied compound. This is due to the fact that the polarizability of Ag^+ ions (d^{10} configuration) is higher than in the case of Na^+. Ag^+ passes more easily through the bottlenecks and consequently more mobile than the Na^+ ions (Belharouak *et al* 2000).
- A larger migration entropy term resulting from a more important disorder in Ag-metal than for AgNa-metal and Na-metal. The increase of entropy term is confirmed by the decrease of parameter (table 2) (Dridi *et al* 2001).

7. Conclusions

The a.c. conductivity and dielectric behaviour of the $Na_2ZnP_2O_7$ compound have been studied as a function of temperature and frequency and an equivalent electrical circuit of the electrochemical cell has been proposed. The electrical transport is through Na^+ hopping mechanism. A comparison of the electrical properties in $Na_2ZnP_2O_7$, $NaAgZnP_2O_7$ and $Ag_2ZnP_2O_7$ compounds shows that the latter have the higher ionic conductivity and the lower activation energy.

References

Almond D P and West A R 1987 *J. Solid State Ionics* **23** 27

Anantha P S and Hariharan K 2005 *J. Mater. Sci. & Eng.* **B121** 12

Ben Rhaiem A, Hlel F, Guidara K and Gargouri M 2009a *J. Alloy. Compd.* **485** 718

Ben Rhaiem A, Chouaib S and Guidara K 2009b *J. Ionics* (accepted)

Ben Rhaiem A, Guidara K, Gargouri M and Daoud A 2005 *J. Alloy. Compd.* **87** 392

Belharouak I, Gravereau P, Parent C, Chaminade J P, Lebraud E and Le Flem G 2000 *J. Solid State Chem.* **152** 466

Chen S A and Liao C S 1993 *J. Macromol.* **26** 2810

Dridi N, Boukhari A, Réau J M, Rbib E and Holt E M 2000 *J. Solid State Ionics* **127** 141

Dridi N, Boukhari A, Réau J M, Rbib E and Holt E M 2001 *J. Mater. Letts.* **47** 212

Erragh F, Boukhari A and Holt E M 1998 *J. Acta Crystallogr.* **C54** 1373

Erragh F, Boukhari A, Eloudi B and Abraham F 1995 *J. Solid State Chem.* **120** 23

El Maadi A, Boukhari A and Holt E M 1995 *J. Chem. Crystallogr.* **25** 531

Ganguli M, Harish Bhat M and Rao K J 1999 *J. Phys. Chem. Glasses* **40** 297

Ghosh S and Ghosh A 2002 *J. Solid State Ionics* **149** 67

Gómez D and Algría A 2001 *J. Non-Crystallogr. Solids* **287** 246

Hodge L M, Ingram M D and West A R 1976 *J. Electroanal. Chem.* **74** 125

Jarboui A, Ben Rhaiem A, Hlel F, Guidara K and Gargouri M 2010 *J. Ionics* **16** 67

Jonscher A K 1977 *J. Nature* (*London*) **267** 673

Kuhlmann U, Thomsen C, Prokoviev A V, Bullesfeld F, Uhrig E and Assmus W 2001 *J. Physica* **B301** 285

Lenfredi S, Saia P S, Lebullenger R and Hemandes A C 2002 *J. Solid State Ionics* **146** 329

Louati B, Gargouri M, Guidara K and Mhiri T 2005 *J. Phys. Chem. Solids* **66** 762

Mahadevan Pillai V P, Thomas B R, Nayar V and Lii K H 1999 *J. Spectrochim. Acta* **A55** 1809

Nadeem M, Akhtar M J and Khan A Y 2005 *Sol. State Commun.* **134** 431

Padmasree K P, Kanchan D K and Kulkarni A R 2006 *J. Solid State Ionics* **177** 475

Papathanassiou A N 2005 *J. Chem. Solids* **66** 1849

Parathan D K, Samantry B K, Chauthaey R N P and Thakur A K 2005 *J. Mater. Sci. Eng.* **B116** 431

Reau J M, Jun X Y, Senegas J, Le Deit Ch and Poulain M 1997 *J. Solid State Ionics* **95** 191

Santha N, Nayar V and Keresztury G 1993 *J. Spectrochim. Acta* **A49** 47

Sanz F, Parada C, Rojo J M, Ruiz-Valero C and Saez-Puche R 1999 *J. Solid State Chem.* **145** 604

Sural M and Gosh A 2000 *J. Solid State Ionics* **130** 259

Uvarov N F, Hairetdinov E F, Reau J M, Bobe J M, Senegas J and Poulain M 1994 *J. Solid State Ionics* **74** 195